Target Localization Based on Distributed Array Networks with Magnitude-Only Measurements

Zhengyu Wan, Wei Liu and Peter Willett

***Abstract*—The source localization problem based on distributed array networks is formulated into a group sparsity based phase retrieval problem where only the magnitude of received signals is available. Under such a framework, a two-dimensional (2D) localization method is proposed, where unlike traditional methods, random phase errors at array sensors will not affect estimation results. In addition, to deal with the off-grid problem for sparsity based solutions, a model for off-grid bias is proposed and an efficient two-step method is developed accordingly to solve the 2-D off-grid problem. Simulation results show that the proposed solutions can solve the problem effectively.**

***Index Terms*—Distributed array networks, localization, magnitude-only measurements, group sparsity, off-grid.**

I. Introduction

Target or source localization is a very important problem in sensor array signal processing and many methods have been proposed such as those based on received signal strength (RSS) [1], [2], time of arrival (TOA) [3], time difference of arrival (TDOA) [4]–[6], direct position determination (DPD) [7], [8] and angle of arrival (AOA) [9], [10].

For AOA based methods, a structure with multiple sensor arrays distributed in a two-dimensional (2-D) space is employed, where synchronization among all distributed sensor arrays is not required. There are normally two steps: the first is applying existing direction of arrival (DOA) estimation methods such as those proposed in [11]–[13] to estimate AOAs at all distributed sensor arrays, while the second is to find intersections of those estimated AOAs in order to localize the sources [9], [10]. Recently, in [14], with the distributed array network, information across all sensor arrays is jointly exploited and the source localization problem was re-formulated into a sparsity maximization problem, where the area of interest in a 2-D Cartesian system is divided into grids along the x-axis and y-axis; under such a framework, a common spatial sparsity support corresponding to all distributed sensor arrays is enforced, leading to a better estimation performance, which also avoids the possible pairing and ambiguity problems associated with a two-step AOA based solution.

The above AOA and sparsity based methods have assumed that there are no phase errors in the array model. In real applications, however, the phase information may not be reliable due to various reasons, and in the extreme case, the phase information may be lost completely, which unavoidably leads to an inaccurate estimation result. On the other hand, inspired by the work in non-coherent (i.e. magnitude-only measurements) DOA estimation, where only magnitude information is captured at all sensors [15]–[22], an non-coherent source localization problem has been proposed in our earlier conference publication [23]. The ambiguities associated with non-coherent measurements at each sub-array is resolved by employing a uniform circular array (UCA) [24]; otherwise, some reference source signals may be needed to remove the resultant ambiguities [16], [21].

One problem associated with the sparsity based estimation approach is that the source locations are implicitly assumed to fall on the discrete grid points. However, in practice, quite often the assumption would not be satisfied, which leads to an off-grid problem. A straightforward solution is to employ a sufficiently dense grid so that the assumption can be considered to be valid to a great degree. However, this will increase the complexity significantly. Another solution is grid refinement, where instead of creating a dense grid initially to alleviate the off-grid problem, a coarse grid is firstly made, and then a denser grid is built around the estimated locations/directions for more accurate estimation. Such a strategy works well, but still incurs a large amount of additional computations. An alternative is to develop solutions which can estimate the grid bias directly, such as those proposed for off-grid DOA estimation in [24]–[28]. To our best knowledge, the off-grid source localization problem have not been addressed yet under the framework of sparsity maximization. In order to deal with the challenge, a two-step off-grid source localization method is also developed. In the first step, the source locations are roughly estimated with a coarser grid, while in the second step, their off-grid bias is estimated through an iterative process, which has a closed-form solution at each iteration. As a performance benchmark, the Cramér-Rao Bound (CRB) is also derived. As demonstrated by computer simulations, compared to the grid refinement method, the proposed one can provide a better result with a lower computational complexity in terms of running time.

The main contributions can be summarized as follows: 1) the target localization problem with magnitude-only measurements is formulated into a group sparsity based phase retrieval problem, where the measurements at all arrays are exploited simultaneously by enforcing the common spatial sparsity; 2) to reduce the computational complexity, an off-grid estimation step is further introduced, where the off-grid biases of both x-

This work is supported by the UK Engineering and Physical Sciences Research Council under grant EP/V009419/1.

Z. Y. Wan and W. Liu are with the Communications Research Group, Department of Electronic and Electrical Engineering,University of Sheffield, Sheffield S1 3JD, UK. P. Willett is with the Department of Electrical and Computer Engineering, University of Connecticut, US. W. Liu is the corresponding author (e-mail: w.liu@sheffield.ac.uk).

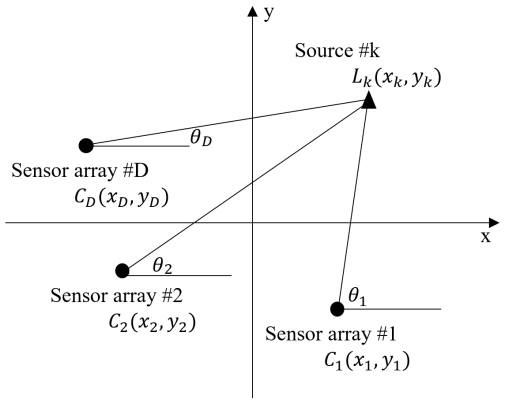

Fig. 1. Source localization geometry.

axis and y-axis are approximated by Taylor series expansion with two variables. As a result, the proposed method does not require synchronization among different subarrays and it works on magnitude-only measurements, which leads to a robust solution where sensor phase errors have no effect on its performance, as also verified by simulations.

The remaining part is structured as follows. The array network model is described in Sec. II, and the proposed solution is presented in Sec. III. Simulation results are provided in Sec. IV and conclusions drawn in Sec. V.

II. Signal model with distributed sensor arrays

Consider K narrowband sources located at Cartesian coordinates $L_k(x_k, y_k)$, $k = 1, ..., K$, impinging on D deployed sensor arrays with coordinates $C_d(x_d, y_d)$, as shown in Fig. 1. The number of sensors at the d-th sensor array is M_d, and the corresponding non-coherent measurements is expressed as

$$\mathbf{Z}_d = |\mathbf{A}_d \mathbf{S}_d| + \mathbf{N}_d, \tag{1}$$

with $\mathbf{S}_d = [\mathbf{s}_d[1], ..., \mathbf{s}_d[P]]$ and $\mathbf{s}_d[p] = [s_{d,1}[p], ..., s_{d,K}[p]]^T$, where $s_{d,k}[p]$ represents the p-th snapshot of the k-th signal, $\mathbf{N}_d$ is the $M_d \times P$ random Gaussian noise vector at the d-th array, $|\cdot|$, and $[\cdot]^T$ are the element-wise absolute value operator and matrix transpose operator, separately, and

$$\mathbf{A}_d = [\mathbf{a}(\theta_{d,1}), ..., \mathbf{a}(\theta_{d,K})] \tag{2}$$

is the steering matrix with its columns $\mathbf{a}(\theta_{d,k})$, $k = 1, ..., K$, being the corresponding steering vectors. When employing a uniform circular array, $\mathbf{a}(\theta_{d,k})$ is given by [29]

$$\mathbf{a}(\theta_{d,k}) = [e^{-j\frac{2\pi r}{\lambda}\cos(\theta_{d,k}-\gamma_1)}, ..., e^{-j\frac{2\pi r}{\lambda}\cos(\theta_{d,k}-\gamma_{M_d})}]^T, \tag{3}$$

where $\gamma_m = 2\pi m/M_d$, λ is wavelength of the signals, r is radius of the circular array, and $\theta_{d,k}$ denotes the arriving angle between the k-th source and d-th array, expressed as

$$\theta_{d,k} = \arctan2(\Delta y_{d,k}, \Delta x_{d,k}), \tag{4}$$

with $\Delta y_{d,k} = y_k - y_d$, $\Delta x_{d,k} = x_k - x_d$, and $\arctan2(\cdot)$ being the inverse four-quadrant tangent operator.

For D distributed arrays, the measurements can be jointly expressed as

$$\mathbf{Z} = |\mathbf{A}\mathbf{S}| + \mathbf{N}, \quad \mathbf{A} = \text{blkdiag}\{\mathbf{A}_1, ..., \mathbf{A}_D\}, \tag{5}$$

where $\text{blkdiag}\{\cdot\}$ generates a block diagonal matrix from its entries, $\mathbf{S} = [\mathbf{s}[1], ..., \mathbf{s}[P]]$, with $\mathbf{s}[p] = [\mathbf{s}_1[p]^T, .., \mathbf{s}_D^T[p]]^T$, and $\mathbf{N} = [\mathbf{N}_1^T, ..., \mathbf{N}_D^T]^T$.

Note that, magnitude-only measurements suffer from some ambiguities, and two of them affect the AOA estimation results: one is mirroring and the other is spatial shift [16], [17], [19], [21]. The mirroring ambiguity refers to the phenomenon that signals arriving from $-\theta_{d,k}$ will generate the measurements with the same magnitude, while for spatial shift ambiguity, it refers to that all estimated arriving angles at the array are phase shifted by a specific amount. However, as shown in [24], while applying a UCA structure, those ambiguities would not appear if the valid DOA range is limited within the range of 180 degrees and therefore UCAs are employed in this work.

By dividing the admissible area of interest into G_x and G_y grids along the x-axis and y-axis in the Cartesian coordinate system, separately, the overcomplete steering matrix of the d-th array can be expressed as

$$\tilde{\mathbf{A}}_d = [\mathbf{a}(\theta_{d,1}), \ldots, \mathbf{a}(\theta_{d,G})], \tag{6}$$

where $\theta_{d,g}$, $g = (g_x - 1)G_x + g_y \in \{1, ..., G = G_x G_y\}$ is the angle between location (x_{g_x}, y_{g_y}) and the d-th array, with

$$\theta_{d,g} = \arctan2(\Delta y_{d,g_y}, \Delta x_{d,g_x}), \tag{7}$$

where $\Delta y_{d,g_x} = y_{g_x} - y_d$, $\Delta x_{d,g_y} = x_{g_y} - x_d$. Accordingly, the d-th array measurements (1) are changed to

$$\mathbf{Z}_d = |\tilde{\mathbf{A}}_d \tilde{\mathbf{S}}_d| + \mathbf{N}_d, \tag{8}$$

where $\tilde{\mathbf{S}}_d = [\tilde{\mathbf{s}}_d[1], ..., \tilde{\mathbf{s}}_d[P]]$ is the sparse signal matrix with K rows corresponding to the targets being non-zero valued, and $\tilde{\mathbf{s}}_d[p]$ represents the corresponding sparse signal vector at the p-th snapshot with only K out of G entries being non-zero valued. Accordingly, a $(\sum_{d=1}^{D} M_d) \times DG_xG_y$ steering matrix $\tilde{\mathbf{A}}$ covering all D sensor arrays can be constructed and the array measurements are given by

$$\mathbf{Z} = |\tilde{\mathbf{A}}\tilde{\mathbf{S}}| + \mathbf{N}, \quad \tilde{\mathbf{A}} = \text{blkdiag}\{\tilde{\mathbf{A}}_1, ..., \tilde{\mathbf{A}}_D\}, \tag{9}$$

where $\tilde{\mathbf{S}} = [\tilde{\mathbf{s}}[1], ..., \tilde{\mathbf{s}}[P]]$ is the joint signal matrix, with $\tilde{\mathbf{s}}[p] = [\tilde{\mathbf{s}}_1[p]^T, .., \tilde{\mathbf{s}}_D^T[p]]^T$.

III. Proposed method

A. Off-Grid Signal Model

In practice, targets may not lay on a pre-defined grid, leading to the off-grid problem. For the d-th array, the steering vector corresponding to the real impinging angle $\theta_{d,k} \notin \{\theta_{d,1}, \ldots, \theta_{d,G}\}$ can be approximated around its nearest on-grid angle θ_{d,g_k} by first-order Taylor expansion as [25]–[27]

$$\begin{aligned} \mathbf{a}(\theta_{d,k}) &\approx \mathbf{a}(\theta_{d,g_k}) + \mathbf{b}(\theta_{d,g_k})(\theta_{d,k} - \theta_{d,g_k}) \\ &\approx \mathbf{a}(\theta_{d,g_k}) + \mathbf{b}(\theta_{d,g_k})\beta_{d,k}, \end{aligned} \tag{10}$$

where $\beta_{d,k}$ denotes the off-gird bias and $\mathbf{b}(\theta_{d,g_k})$ is the derivative of $\mathbf{a}(\theta_{d,g_k})$.

For source localization, the true AOA at the d-th array $\theta_{d,k}$ is a function of two variables $(\Delta y_{d,g_y}, \Delta x_{d,g_x})$, determined by two unknown variables x_k and y_k, as presented

in Eqs. (6-8). As a result, while $x_k \notin \{x_1, \ldots, x_{G_x}\}$ and $y_k \notin \{y_1, \ldots, y_{G_y}\}$, the steering vector of the d-th array corresponding to the real source location can be approximated around its nearest on-grid location $(x_{g_k},\ y_{g_k})$ by first-order Taylor expansion of two variables as

$$\begin{aligned}\mathbf{a}(\theta_{d,k}) &\approx \mathbf{a}(\theta_{d,k}) + \mathbf{b}_x(\theta_{d,k})(\Delta x_{d,k} - \Delta x_{d,g_k}) \\ &\quad + \mathbf{b}_y(\theta_{d,k})(\Delta y_{d,k} - \Delta y_{d,g_k}) \\ &\approx \mathbf{a}(\theta_{d,k}) + \mathbf{b}_x(\theta_{d,k})\beta_{k,x} + \mathbf{b}_y(\theta_{d,k})\beta_{k,y},\end{aligned} \tag{11}$$

where $\beta_{k,x}$ and $\beta_{k,y}$ represent the off-gird biases with respect to x-axis and y-axis, separately, while $\mathbf{b}_x(\theta_{d,g}) = \frac{\partial \mathbf{a}(\theta_{d,g})}{\partial x_g}$ and $\mathbf{b}_y(\theta_{d,g}) = \frac{\partial \mathbf{a}(\theta_{d,g})}{\partial y_g}$ are the partial derivatives of $\mathbf{a}(\theta_{d,k})$.

Let $\mathbf{x} = [x_1, ..., x_K]$ and $\mathbf{y} = [y_1, ..., y_K]$ denote the true locations of K sources, and (8) can be approximated by the first order approximation of two variables, given by

$$\mathbf{Z}_d \approx |(\tilde{\mathbf{A}}_d + \tilde{\mathbf{B}}_{d,x}\boldsymbol{\Delta}_x + \tilde{\mathbf{B}}_{d,y}\boldsymbol{\Delta}_y)\tilde{\mathbf{S}}_d| + \mathbf{N}_d, \tag{12}$$

with $\mathbf{B}_{d,x} = [\mathbf{b}_x(\theta_{d,1}), ..., \mathbf{b}_x(\theta_{d,G})]$, $\boldsymbol{\Delta}_x = \mathrm{diag}(\boldsymbol{\beta}_x)$ and $\boldsymbol{\beta}_x = [\beta_{1,x}, ..., \beta_{G,x}]$, where

$$\beta_{g,x} = \begin{cases} \bar{x}_k - x_{g_x}, & \text{if } g = g_k, \\ 0, & \text{otherwise.} \end{cases} \tag{13}$$

Similarly, we have $\tilde{\mathbf{B}}_{d,y} = [\mathbf{b}_y(\theta_{d,1}), ..., \mathbf{b}_y(\theta_{d,G})]$, $\boldsymbol{\Delta}_y = \mathrm{diag}(\boldsymbol{\beta}_y)$ and $\boldsymbol{\beta}_y = [\beta_{1,y}, ..., \beta_{G,y}]$, where

$$\beta_{g,y} = \begin{cases} \bar{y}_k - x_{g_y}, & \text{if } g = g_k, \\ 0, & \text{otherwise.} \end{cases} \tag{14}$$

$\beta_{g,x}$ and $\beta_{g,y}$ satisfy $-\frac{v_x}{2} \le \beta_{g,x} \le \frac{v_x}{2}$ and $-\frac{v_y}{2} \le \beta_{g,y} \le \frac{v_y}{2}$, separately, where v_x and v_y are grid stepsizes with respect x-axis and y-axis, respectively.

Noted that, sources from an arbitrary grid point in the Cartesian coordinate system would share the same spatial support of $\tilde{\mathbf{A}}_d$, $d = 1, ..., D$, although the arriving angles with respect to different arrays are different. Therefore, the source localization problem can be formulated as a joint group sparsity based optimization problem, given by

$$\min_{\tilde{\mathbf{S}}, \boldsymbol{\beta}_x, \boldsymbol{\beta}_y} \|\mathbf{Z} - |(\tilde{\mathbf{A}} + \tilde{\mathbf{B}}_x\tilde{\boldsymbol{\Delta}}_x + \tilde{\mathbf{B}}_y\tilde{\boldsymbol{\Delta}}_y)\tilde{\mathbf{S}}|\|_F^2 + \rho\|\hat{\mathbf{S}}\|_{2,1}, \tag{15}$$

where

$$\begin{aligned}\hat{\mathbf{S}} &= [\tilde{\mathbf{S}}_1, \ldots, \tilde{\mathbf{S}}_D], \\ \tilde{\mathbf{B}}_x &= \mathrm{blkdiag}\{\tilde{\mathbf{B}}_{1,x}, ..., \tilde{\mathbf{B}}_{D,x}\}, \\ \tilde{\mathbf{B}}_y &= \mathrm{blkdiag}\{\tilde{\mathbf{B}}_{1,y}, ..., \tilde{\mathbf{B}}_{D,y}\}, \\ \tilde{\boldsymbol{\Delta}}_x &= \mathrm{blkdiag}\{\boldsymbol{\Delta}_x, ..., \boldsymbol{\Delta}_x\}, \\ \tilde{\boldsymbol{\Delta}}_y &= \mathrm{blkdiag}\{\boldsymbol{\Delta}_y, ..., \boldsymbol{\Delta}_y\},\end{aligned} \tag{16}$$

with $\|\cdot\|_{2,1}$ and $\|\cdot\|_F$ represent $l_{2,1}$ norm and Frobenius norm, respectively. The $l_{2,1}$ norm is defined as

$$\|\hat{\mathbf{S}}\|_{2,1} := \sum_{g=1}^{G} \|\hat{\mathbf{s}}_g\|_2, \tag{17}$$

with $\hat{\mathbf{s}}_g$ being the g-th row vector of $\hat{\mathbf{S}}$. As a result, $\hat{\mathbf{S}}$ contains $G = G_xG_y$ groups and the g-th group, $g \in \{1, ..., G\}$, is a $1 \times DP$ vector, consisting of g-th row vectors of all $\tilde{\mathbf{S}}_d$, $d \in \{1, .., D\}$.

B. Proposed Method

First, for the on-grid solution, i.e. the off-grid biases $\tilde{\boldsymbol{\Delta}}_x$ and $\tilde{\boldsymbol{\Delta}}_y$ are assumed to be zero, and the corresponding optimization problem in (15) is simplified to

$$\min_{\tilde{\mathbf{S}}} \|\mathbf{Z} - |\tilde{\mathbf{A}}\tilde{\mathbf{S}}|\|_F^2 + \rho\|\hat{\mathbf{S}}\|_{2,1}. \tag{18}$$

The above formulation has the same form as those considered in group sparsity based phase retrieval problem for DOA estimation, which can be solved by the algorithm ToyBar [21].

For the general off-grid case, instead of jointly estimate $\tilde{\boldsymbol{\Delta}}_x$, $\tilde{\boldsymbol{\Delta}}_y$ and $\tilde{\mathbf{S}}$ in (15), this problem is solved iteratively. In the first step, we employ (18) to find the rough grid locations of targets.

In the second step, the PRIME technique [30] is employed, and the first term of (15) without off-grid bias at the p-th snapshot is reformulated as

$$\begin{aligned}&\min_{\tilde{\mathbf{s}}} \sum_{m=1}^{M} (|\tilde{\mathbf{a}}_m\tilde{\mathbf{s}}[p]|^2 - 2z_m[p]|\tilde{\mathbf{a}}_m\tilde{\mathbf{s}}[p]| + |z_m[p]|^2) \\ &= \min_{\tilde{\mathbf{s}}} \sum_{m=1}^{M} (|\tilde{\mathbf{a}}_m\tilde{\mathbf{s}}[p]|^2 - 2z_m[p]|\tilde{\mathbf{a}}_m\tilde{\mathbf{s}}[p]|),\end{aligned} \tag{19}$$

where $\tilde{\mathbf{a}}_m$ represents the m-th row of the steering matrix $\tilde{\mathbf{A}}$, and $z_m[p]$ is the m-th element of $\mathbf{z}[p]$. Since

$$\mathrm{Re}(\tilde{\mathbf{a}}_m\tilde{\mathbf{s}}[p](\tilde{\mathbf{s}}^q[p])^H\tilde{\mathbf{a}}_m^H) \le |\tilde{\mathbf{a}}_m\tilde{\mathbf{s}}[p]||\tilde{\mathbf{a}}_m\tilde{\mathbf{s}}^q[p]|, \tag{20}$$

where $\mathrm{Re}(\cdot)$ represents the real part and the equality is met while $\tilde{\mathbf{s}}[p] = \tilde{\mathbf{s}}^q[p]$, it can be majorized as

$$\min_{\tilde{\mathbf{s}}} \sum_{m=1}^{M} (|\tilde{\mathbf{a}}_m\tilde{\mathbf{s}}[p]|^2 - 2|z_m[p]|\frac{\mathrm{Re}(\tilde{\mathbf{a}}_m\tilde{\mathbf{s}}[p](\tilde{\mathbf{s}}^q[p])^H\mathbf{a}_m^H)}{|\tilde{\mathbf{a}}_m\tilde{\mathbf{s}}^q[p]|}), \tag{21}$$

which can be formulated as

$$\min_{\tilde{\mathbf{s}}} \ \|\tilde{\mathbf{A}}\tilde{\mathbf{s}}[p] - \mathbf{c}^q[p]\|_2^2, \quad \text{with} \quad \mathbf{c}^q[p] = \mathbf{y} \odot e^{j\arg(\tilde{\mathbf{A}}\tilde{\mathbf{s}}^q[p])}, \tag{22}$$

where $\odot$ denotes the Hadamard product, $\tilde{\mathbf{s}}^q$ is a known complex vector and $\arg(\cdot)$ represents the phase applied element-wise. Consider the off-grid biases, the PRIME technique is applied column by column to the first term of (15), and the corresponding objective function is changed to

$$\min_{\boldsymbol{\beta}_x, \boldsymbol{\beta}_y} \ \|(\tilde{\mathbf{A}} + \tilde{\mathbf{B}}_x\tilde{\boldsymbol{\Delta}}_x + \tilde{\mathbf{B}}_y\tilde{\boldsymbol{\Delta}}_y)\tilde{\mathbf{S}} - \bar{\mathbf{C}}\|_F^2 + \rho\|\hat{\mathbf{S}}\|_{2,1}, \tag{23}$$

with $\bar{\mathbf{C}} = \mathbf{Z} \odot e^{j\arg(\tilde{\mathbf{A}}\tilde{\mathbf{S}}_e)}$, where $\tilde{\mathbf{S}}_e$ is estimated signals from step one, which is susceptible to global phase ambiguity.

After that, an iterative algorithm for estimating dictionary bias $\tilde{\boldsymbol{\beta}}$ is proposed. This method first estimates K non-zero rows of estimated signals $\tilde{\mathbf{S}}_K^i$ as

$$\bar{\boldsymbol{S}}_K^i = (\bar{\boldsymbol{A}}_K^i)^\dagger\bar{\mathbf{C}}, \tag{24}$$

where $(\cdot)^\dagger$ is the pseudo-inverse operator, $i \in \{1, ..., I\}$ is iteration index, $\bar{\boldsymbol{A}}_K^i$ is the steering matrix with K columns corresponding to the estimated source locations, given by

$$\begin{aligned}\bar{\mathbf{A}}_K^i &= \mathrm{blkdiag}\{\bar{\mathbf{A}}_{1,K}^i, ..., \bar{\mathbf{A}}_{D,K}^i\}, \\ \bar{\mathbf{A}}_{d,K}^i &= [\mathbf{a}(\theta_{d,1}^i), ..., \mathbf{a}(\theta_{d,K}^i)],\end{aligned} \tag{25}$$

and $\theta^i_{d,K}$ is updated with x^i and y_i obtained from the previous iteration. x^0 and y^0 is initialized as K columns of $\tilde{\mathbf{A}}_d$, which corresponds to locations of estimated sources $\tilde{\mathbf{S}}_e$. As the biases $\tilde{\boldsymbol{\beta}}_x$ and $\tilde{\boldsymbol{\beta}}_y$ share the same support with $\tilde{\mathbf{S}}_e$, $\bar{\mathbf{B}}_{d,x}$ and $\bar{\mathbf{B}}_{d,y}$ are obtained, which are the sub-matrix of $\tilde{\mathbf{B}}_{d,x}$ and $\tilde{\mathbf{B}}_{d,y}$. Similarly, the biases of corresponding source locations $\bar{\boldsymbol{\Delta}}^i_{K,x} = \mathrm{diag}(\bar{\boldsymbol{\beta}}^i_x) = [\beta^i_{1,x}, ...\beta^i_{K,x}]^T$ and $\bar{\boldsymbol{\Delta}}^i_{K,y} = \mathrm{diag}(\bar{\boldsymbol{\beta}}^i_y) = [\beta^i_{1,y}, ...\beta^i_{K,y}]^T$ are obtained.

By denoting $\bar{\mathbf{B}}^i_x = \mathrm{blkdiag}\{\mathbf{B}^i_{1,x}, ..., \mathbf{B}^i_{D,x}\}$, $\bar{\mathbf{B}}^i_y = \mathrm{blkdiag}\{\mathbf{B}^i_{1,y}, ..., \mathbf{B}^i_{D,y}\}$, $\bar{\boldsymbol{\Delta}}^i_x = \mathrm{blkdiag}\{\bar{\boldsymbol{\Delta}}^i_{K,x}, ..., \bar{\boldsymbol{\Delta}}^i_{K,x}\}$, and $\bar{\boldsymbol{\Delta}}^i_y = \mathrm{blkdiag}\{\bar{\boldsymbol{\Delta}}^i_{K,y}, ..., \bar{\boldsymbol{\Delta}}^i_{K,y}\}$, the off-grid biases can be estimated by solving

$$\min_{\bar{\boldsymbol{\beta}}_x, \bar{\boldsymbol{\beta}}_y} \|(\bar{\mathbf{A}}^i_K + \bar{\mathbf{B}}^i_{d,x}\bar{\boldsymbol{\Delta}}^i_x + \bar{\mathbf{B}}^i_{d,y}\bar{\boldsymbol{\Delta}}^i_y)\bar{\mathbf{S}}^i_K - \bar{\mathbf{C}}\|^2_F. \tag{26}$$

Once the PRIME technique is done, this process updates each off-grid bias $\bar{\boldsymbol{\beta}}_x$ and $\bar{\boldsymbol{\beta}}_y$ in (26) at a time.

Firstly, with $\bar{\beta}^i_y$ fixed to zero, $\bar{\beta}^i_x$ is pursued by solving

$$\min_{\bar{\boldsymbol{\beta}}_x} \|(\bar{\mathbf{A}}^i_K + \bar{\mathbf{B}}^i_x\bar{\boldsymbol{\Delta}}^i_x)\bar{\mathbf{S}}^i_K - \bar{\mathbf{C}}_d\|^2_F. \tag{27}$$

Since $\bar{\mathbf{A}}^i_K$ and $\bar{\mathbf{B}}^i_x$ are block diagonal, (27) can be reformulated as

$$\min_{\bar{\boldsymbol{\beta}}_x} \sum_{d=1}^{D} \|(\bar{\mathbf{A}}^i_{d,K} + \bar{\mathbf{B}}^i_{d,x}\bar{\boldsymbol{\Delta}}^i_x)\bar{\mathbf{S}}^i_{d,K} - \bar{\mathbf{C}}_d\|^2_F, \tag{28}$$

where $\mathbf{C}_d$ and $\bar{\mathbf{S}}^i_{d,K}$ are the approximated measurements and estimated signals of the d-th subarray. Dropping index i for simplicity, (28) can be approximated as [24]–[26]

$$\begin{aligned}
&\sum_{d=1}^{D}\|(\bar{\mathbf{A}}_{d,K} + \bar{\mathbf{B}}_{d,x}\bar{\boldsymbol{\Delta}}_K)\bar{\mathbf{S}}_{d,K} - \bar{\mathbf{C}}_d\|^2_F \\
&\quad\approx \sum_{d=1}^{D}\Big\{\bar{\boldsymbol{\beta}}^T_x\big(\bar{\mathbf{B}}^H_{d,x}\bar{\mathbf{B}}_{d,x} \odot (\bar{\mathbf{S}}_{d,K}\bar{\mathbf{S}}^H_{d,K})^*\big)\bar{\boldsymbol{\beta}}_x \\
&\quad\quad - 2\mathrm{Re}\{\mathrm{diag}[\bar{\mathbf{S}}_{d,K}(\bar{\mathbf{C}}_d - \bar{\mathbf{A}}_K\bar{\mathbf{S}}_{d,K})^H\bar{\mathbf{B}}_{d,x}]\bar{\boldsymbol{\beta}}_x\}\Big\},
\end{aligned} \tag{29}$$

where $\mathrm{tr}(\cdot)$ and $\mathrm{Re}(\cdot)$ represent the trace and real part of its variable, separately. The optimal condition, $\bar{\boldsymbol{\beta}}^i_x$ can be obtained by

$$\begin{aligned}
&\bar{\boldsymbol{\beta}}^{i+1}_x = \mathrm{Re}\{(\mathbf{J}^i_x)^{-1}\mathbf{h}^i\}, \mathbf{J}^i_x = \sum_{d=1}^{D}\mathbf{J}^i_{d,x},\ \mathbf{h}_x = \sum_{d=1}^{D}\mathbf{h}^i_{d,x}, \\
&\mathbf{J}^i_{d,x} = (\mathbf{B}^i_{d,x})^H\bar{\mathbf{B}}^i_{d,x} \odot (\bar{\mathbf{S}}^i_{d,K}\bar{\mathbf{S}}^i_{d,K})^*, \\
&\mathbf{h}^i_{d,x} = \big\{\mathrm{diag}[\bar{\mathbf{S}}^i_{d,K}(\bar{\mathbf{C}}_d - \bar{\mathbf{A}}^i_{d,K}\bar{\mathbf{S}}^i_{d,K})^H\bar{\mathbf{B}}^i_{d,x}]\big\}^T.
\end{aligned} \tag{30}$$

where $(\cdot)^{-1}$ is the inverse operator. While the off-grid bias with respect to x-axis is fixed, the off-grid bias of the y-axis $\boldsymbol{\beta}_y$ can be obtained by

$$\min_{\bar{\boldsymbol{\beta}}_y} \sum_{d=1}^{D} \|(\bar{\mathbf{A}}^i_{d,K} + \bar{\mathbf{B}}^i_{d,x}\bar{\boldsymbol{\Delta}}^i_x + \bar{\mathbf{B}}^i_{d,y}\bar{\boldsymbol{\Delta}}^i_y)\bar{\mathbf{S}}^i_{d,K} - \bar{\mathbf{C}}_d\|^2_F. \tag{31}$$

Similarly, we have

$$\begin{aligned}
&\bar{\boldsymbol{\beta}}^i_y = \mathrm{Re}\{(\mathbf{J}^i_y)^{-1}\mathbf{h}^i_y\}, \mathbf{J}^i_y = \sum_{d=1}^{D}\mathbf{J}^i_{d,y},\ \mathbf{h}^i_y = \sum_{d=1}^{D}\mathbf{h}^i_{d,y}, \\
&\mathbf{J}^i_{d,y} = (\mathbf{B}^i_{d,y})^H\bar{\mathbf{B}}^i_{d,y} \odot (\bar{\mathbf{S}}^i_{d,K}\bar{\mathbf{S}}^i_{d,K})^*, \\
&\mathbf{h}^i_{d,y} = \big\{\mathrm{diag}[\bar{\mathbf{S}}^i_{d,K}(\bar{\mathbf{C}}_d - (\bar{\mathbf{A}}^i_{d,K} + \mathbf{B}^{i+1}_{d,x}\bar{\boldsymbol{\Delta}}^{i+1}_x)\bar{\mathbf{S}}^i_{d,K})^H\bar{\mathbf{B}}^i_{d,y}]\big\}^T.
\end{aligned} \tag{32}$$

Note that, the non-coherent DOA estimation results still suffer from the global phase ambiguity, that is

$$\begin{aligned}
\bar{\mathbf{C}} &= \mathbf{Z} \odot e^{j\arg(\tilde{\mathbf{A}}\tilde{S}_e)} \approx \mathbf{A}_r\mathbf{S}_r e^{j\phi}, \\
\bar{\mathbf{S}}_K &= (\bar{\boldsymbol{A}}^i_K)^\dagger\bar{\mathbf{C}} \approx \mathbf{S}_r e^{j\phi},
\end{aligned} \tag{33}$$

where $\mathbf{S}_r$ and $\mathbf{A}_r$ represent the real signal and its corresponding real steering matrix, respectively, and ϕ is a global phase factor. It can be seen that, when substituting (33) into (30) and (32), the global phase factor cancels, which means that the global phase ambiguity will not affect bias estimation in this step.

With $\bar{\boldsymbol{\beta}}^i_x$ and $\bar{\boldsymbol{\beta}}^i_y$, the steering matrix $\mathbf{A}_{d,K}$ is updated as

$$x^{i+1}_k = x^i_k + \boldsymbol{\beta}^i_{k,x},\ y^{i+1}_k = y^i_k + \boldsymbol{\beta}^i_{k,y}, \tag{34}$$

where $\beta_{k,x}$ and $\beta_{k,y}$ represent the bias of the k-th source, $x^0_{d,k}$ and $y^0_{d,k}$ are the initial locations obtained from the first step, i.e corresponding locations of $\tilde{\boldsymbol{S}}_e$. Finally, the estimated locations of the k-th source can be obtained after I iterations.

The full algorithm is summarized in the Algorithm Summary table.

Algorithm Summary (Two-Step Off-Grid)

Input: $\tilde{\mathbf{A}}$, $\mathbf{Z}$,
Initializtion: $\bar{\boldsymbol{\beta}}^0_x = \mathbf{0}$, $\bar{\boldsymbol{\beta}}^0_y = \mathbf{0}$.
Step 1: Estimate $\tilde{\mathbf{S}}_e$ via existing group sparse phase retrieval algorithms
Obtain $\bar{\boldsymbol{A}}^0_K$, $\mathbf{x}^0$ and $\mathbf{y}^0$
Calculate $\bar{\mathbf{C}} = \mathbf{Z} \odot e^{j\arg(\tilde{\mathbf{A}}\tilde{\mathbf{S}}_e)}$.
Step 2: for i=1, ..., I
1) Calculate $\bar{\mathbf{S}}^i_K = (\bar{\boldsymbol{A}}^i_K)^\dagger\bar{\mathbf{C}}$.
2) Calculate $\bar{\boldsymbol{\beta}}^i_x = \mathrm{Re}\{(\mathbf{J}^i_x)^{-1}\mathbf{h}^i\}$ from (30)
3) Restrict elements of $\bar{\boldsymbol{\beta}}^i_x$ within range $[-\frac{v_x}{2}, \frac{v_x}{2}]$.
4) Calculate $\bar{\boldsymbol{\beta}}^i_y = \mathrm{Re}\{(\mathbf{J}^i_y)^{-1}\mathbf{h}^i\}$ from (32)
5) Restrict elements of $\bar{\boldsymbol{\beta}}^i_y$ within range $[-\frac{v_y}{2}, \frac{v_y}{2}]$.
6) Calculate $\mathbf{x}^{i+1} = \mathbf{x}^i + \boldsymbol{\beta}^i_x,\ \mathbf{y}^{i+1} = y^i + \boldsymbol{\beta}^i_y$
7) $\bar{\mathbf{A}}^{i+1}_{d,K} = \bar{\mathbf{A}}_K(\boldsymbol{\theta}^{i+1}_d)$.
Output localization results: $\mathbf{x}^i,\ \mathbf{y}^i$.

C. Cramér-Rao Bound (CRB)

From (5), the probability density function is expressed as

$$p(\mathbf{Z}; \boldsymbol{\Phi}) = \prod_{p=1}^{P}\prod_{m=1}^{M}\frac{1}{2\pi\sigma^2_m}e^{(z_m[p] - |\mathbf{a}_m\mathbf{s}[p]|)^2/2\sigma^2_m}, \tag{35}$$

where $M = \sum_{d=1}^{D} M_d$, $\mathbf{a}_m$ is the m-th row of $\mathbf{A}$, $z_m[p]$ represents the m-th entry of $\mathbf{Z}$ at the p-th snapshot and σ_m is noise power.

Since the reconstructed signals are up to a global phase factor, for complex signals, the Fisher information matrix (FIM) would be singular [31]. Thus, similar to [21], instead of estimating the phase information of signals, only phase differences between signals are considered. Assuming the

noise level at all distributed sensor arrays are identical, the unknown parameter vector of arriving angles, magnitude, phase difference and noise level can be represented as

$$\begin{aligned}\boldsymbol{\Phi} &= [\mathbf{L}_x^T, \mathbf{L}_y^T, |\boldsymbol{s}[p]|, \boldsymbol{\Delta\gamma}[p], \sigma_m^2]^T \\ \mathbf{L}_x &= [x_1, ..., x_K]^T,\ \mathbf{L}_y = [y_1, ..., y_K]^T, \\ |\boldsymbol{s}[p]| &= [|\boldsymbol{s}_1^T[p]|, ..., |\boldsymbol{s}_D^T[p]|]^T, \\ \boldsymbol{\Delta\gamma}[p] &= [\boldsymbol{\Delta\gamma}_1^T[p], ..., \boldsymbol{\Delta\gamma}_D^T[p]]^T, \\ \boldsymbol{\Delta\gamma}_d[p] &= [\Delta\gamma_{12,d}[p], \Delta\gamma_{13,d}[p], ..., \Delta\gamma_{(K-1)K,d}[p]]^T,\end{aligned} \tag{36}$$

where $\boldsymbol{\Delta\gamma}_d[p]$ contains $(K^2-K)/2$ entries, $\Delta\gamma_{kk',d}[p] = \gamma_{k,d}[p] - \gamma_{k',d}[p]$, $\gamma_{k,d}[p]$ is the phase of the k-th signal of the d-th sensor array at the p-th snapshot and σ_m^2 is noise power.

For the deterministic model, the FIM $\mathbf{F}$ is defined as [32]

$$\mathbf{F} = \mathbb{E}\{\frac{\partial \ln^2 p(\mathbf{Z}; \boldsymbol{\Phi})}{\partial \boldsymbol{\Phi} \partial \boldsymbol{\Phi}^T}\} \tag{37}$$

The $\{i,j\}$-th entry of $\mathbf{F}$ is given by [33]

$$\begin{aligned}\mathbf{F}_{i,j} = &\Big[\frac{\partial \boldsymbol{\mu}(\boldsymbol{\Phi})}{\partial \Phi_i}\Big]^T \boldsymbol{\Gamma}^{-1}(\boldsymbol{\Phi}) \Big[\frac{\partial \boldsymbol{\mu}(\boldsymbol{\Phi})}{\partial \Phi_j}\Big] \\ &+ \frac{1}{2}\Big[\boldsymbol{\Gamma}^{-1}(\boldsymbol{\Phi}) \frac{\partial \boldsymbol{\Gamma}^{-1}(\boldsymbol{\Phi})}{\partial \Phi_i} \boldsymbol{\Gamma}^{-1}(\boldsymbol{\Phi}) \frac{\partial \boldsymbol{\Gamma}^{-1}(\boldsymbol{\Phi})}{\partial \Phi_j}\Big],\end{aligned} \tag{38}$$

where $\boldsymbol{\Gamma}^{-1}(\boldsymbol{\Phi}) = \frac{1}{\sigma_m^2}\mathbf{I}_M$, $\mathbf{I}_M$ is the identity matrix, $(\cdot)^{-1}$ is the matrix inverse operator, and $\boldsymbol{\mu}(\boldsymbol{\Phi}) = |\mathbf{AS}|$. Since $\boldsymbol{\mu}(\boldsymbol{\Phi})$ is independent of the noise level, we have

$$\mathbf{F} = \begin{bmatrix}\tilde{\mathbf{F}} & \mathbf{0} \\ \mathbf{0} & \mathbf{0}\end{bmatrix} + \begin{bmatrix}\mathbf{0} & \mathbf{0} \\ \mathbf{0} & \mathbf{F}_{\sigma_m}\end{bmatrix}, \tag{39}$$

As the FIM is block diagonal, $\mathbf{F}_{\sigma_m}$ has no effect on the CRB result of locations. Thus, the location CRB can be determined by the inverse of $\mathbf{F}$. Computing the derivatives of $\boldsymbol{\mu}(\boldsymbol{\Phi})$ with respect to $\boldsymbol{\Phi}$, we have

$$\mathbf{C} = \frac{\partial \boldsymbol{\mu}(\boldsymbol{\Phi})}{\partial \boldsymbol{\Phi}^T} = [\mathbf{G}, \mathbf{H}, \boldsymbol{\Delta}, \mathbf{0}], \tag{40}$$

Denotes $|\mathbf{a}_m\mathbf{s}| = (\mathbf{s}^H\mathbf{a}_m^H\mathbf{a}_m\mathbf{s})^{\frac{1}{2}} = (\mathbf{s}^H\mathbf{A}_m\mathbf{s})^{\frac{1}{2}}$ and drop index p for convenience, the first block of $\mathbf{C}$ is

$$\begin{aligned}\mathbf{G} &= [\mathbf{G}_{1,x}^T, ..., \mathbf{G}_{D,x}^T, \mathbf{G}_{1,y}^T, ..., \mathbf{G}_{D,y}^T]^T, \\ \mathbf{G}_{d,x} &= [\mathbf{g}_{d,1,x}^T, ..., \mathbf{g}_{d,M_d,x}^T]^T, \\ \mathbf{G}_{d,y} &= [\mathbf{g}_{d,1,y}^T, ..., \mathbf{g}_{d,M_d,y}^T]^T, \\ \mathbf{g}_{d,m,x} &= [\frac{\partial|\mathbf{a}_{m,d}\mathbf{s}_d|}{\partial x_1}, ..., \frac{\partial|\mathbf{a}_{m,d}\mathbf{s}_d|}{\partial x_K}], \\ \mathbf{g}_{d,m,y} &= [\frac{\partial|\mathbf{a}_{m,d}\mathbf{s}_d|}{\partial y_1}, ..., \frac{\partial|\mathbf{a}_{m,d}\mathbf{s}_d|}{\partial y_K}],\end{aligned} \tag{41}$$

with

$$\begin{aligned}\frac{\partial|\mathbf{a}_{m,d}\mathbf{s}_d|}{\partial x_k} &= \alpha_{d,x,k}\mathrm{Im}\Big(\xi\sin(\theta_{d,k}-\gamma_m)s_{d,k}^*\mathbf{A}_{m,d}(k,:)\mathbf{s}\Big), \\ \alpha_{d,x,k} &= (\mathbf{s}^H\mathbf{A}_{m,d}\mathbf{s})^{-\frac{1}{2}}\frac{-\Delta y_{d,k}}{\Delta x_{d,k}^2 + \Delta y_{d,k}^2}, \xi = 2\pi r/\lambda, \\ \frac{\partial|\mathbf{a}_{m,d}\mathbf{s}_d|}{\partial y_k} &= \alpha_{d,y,k}\mathrm{Im}\Big(\xi\sin(\theta_{d,k}-\gamma_m)s_{d,k}^*\mathbf{A}_{m,d}(k,:)\mathbf{s}\Big), \\ \alpha_{d,y,k} &= (\mathbf{s}^H\mathbf{A}_{m,d}\mathbf{s})^{-\frac{1}{2}}\frac{\Delta x_{d,k}}{\Delta x_{d,k}^2 + \Delta y_{d,k}^2},\end{aligned} \tag{42}$$

where $(\cdot)^*$ is the complex conjugate operator, $\mathbf{A}_{m,d}(k,:)$ is the k-th row of $\mathbf{A}_{m,d}$ and $\mathbf{A}_{m,d}(:,k)$ is the k-th column of $\mathbf{A}_{m,d}$. The second block is expressed by

$$\begin{aligned}\mathbf{H} &= \frac{\partial|\mathbf{As}|}{\partial|\mathbf{s}^T|} = \mathrm{blkdiag}\{\mathbf{H}_1, ..., \mathbf{H}_D\}, \\ \mathbf{H}_d^T &= \mathrm{Re}\Big(\mathrm{diag}(e^{-j\boldsymbol{\gamma}_d})\mathbf{A}_d^H\mathrm{diag}(\mathbf{A}_d\mathbf{s}_d)]\Big)\tilde{\mathbf{z}}_d, \\ \tilde{\mathbf{z}}_d &= \mathrm{diag}\{|\mathbf{A}_d\mathbf{s}_d|\}^{-\frac{1}{2}}.\end{aligned} \tag{43}$$

Then, the third block is given by

$$\begin{aligned}\boldsymbol{\Delta} &= \frac{\partial|\mathbf{As}|}{\partial|\Delta\boldsymbol{\gamma}^T|} = \mathrm{blkdiag}\{\boldsymbol{\Delta}_1, ..., \boldsymbol{\Delta}_D\}, \\ \boldsymbol{\Delta}_d^T &= -\mathrm{Im}\Big(\mathrm{diag}\{\dot{\mathbf{s}}_d\}\dot{\mathbf{A}}_d \odot \mathrm{diag}\{\ddot{\mathbf{s}}_d\}\ddot{\mathbf{A}}_d\Big)\tilde{\mathbf{z}}_d, \\ \dot{\mathbf{s}}_d &= [\overbrace{s_{d,1}, ..., s_{d,1}}^{K-1}, \overbrace{s_{d,2}..., s_{d,2}}^{K-2}, ..., s_{d,K-1}], \\ \dot{\mathbf{A}}_d &= [\overbrace{\mathbf{A}(:,1)_d^T, ..., \mathbf{A}(:,1)_d^T}^{K-1}, ..., \mathbf{A}(:,K-1)_d^T], \\ \ddot{\mathbf{s}}_d &= [s_{d,2}^*, ..., s_{d,K}^*, s_{d,3}^*, ..., s_{d,K}^*, ..., s_{d,K}^*], \\ \ddot{\mathbf{A}} &= [\mathbf{A}(:,2)_d^H, ..., \mathbf{A}(:,K)_d^H, ..., \mathbf{A}(:,K)_d^H],\end{aligned} \tag{44}$$

where $\odot$ stands for the Hadamard product.

Then, $\tilde{\mathbf{F}}$ can be given by

$$\tilde{\mathbf{F}} = \sum_{p=1}^{P}\frac{1}{\sigma_m^2}\mathbf{C}[p]^H\mathbf{C}[p]. \tag{45}$$

The CRB associated with locations of signals can be obtained by the inverse of $\tilde{\mathbf{F}}$.

IV. Simulations

In this section, simulation results are provided to show the performance of the proposed methods in comparison with the existing sparsity based on-grid method with coherent measurements (with both magnitude and phase information) [14]. For on-grid methods, when grid refinement is employed, it is referred to as the refinement method, while for the off-grid method, the iteration number for the second step is 20. The sparse phase retrieval algorithm ToyBar in [21] is applied in the non-coherent scenario, and the number of iterations before stop is set to 300, with 30 random initialisations used in order to find the global minimum.

The area of interest is set as $[-20, 20]$m along both x-axis and y-axis. In the initial step for both on-grid and off-grid methods, 2m is used as the stepsize for constructing the overcomplete steering matrix $\tilde{\mathbf{A}}$ unless specified otherwise. In the refinement step, a new grid with stepsize 0.2m is formed around a distance of 1m to either side of the estimated location from the initial step. There are $D = 4$ distributed sensor arrays placed at $C_1 = (10, 40)$m, $C_2 = (30, 10)$m, $C_3 = (-80, 90)$m and $C_4 = (-20, 40)$m, while the off-grid locations for $K = 2$ sources are $L_1 = (-10.5, -9.5)$m and $L_2 = (0.5, 12.5)$m. The number of sensors at each distributed sensor array M_d is set as 20, while the radius r of the UCAs is set as $r = \frac{M_d\frac{\lambda}{2}}{2\pi}$, and $P = 100$ snapshots are collected unless specified otherwise.

For the first set of simulations, the signal to noise ratio (SNR) is 20 dB. The spatial spectrum of the proposed non-coherent localization results is shown in Fig. 2, where Fig. 2a provides the result of the on-grid step, while Fig. 2b is for the extra off-grid step. It can be seen that the two sources have been identified successfully, but the off-grid step significantly increases the accuracy.

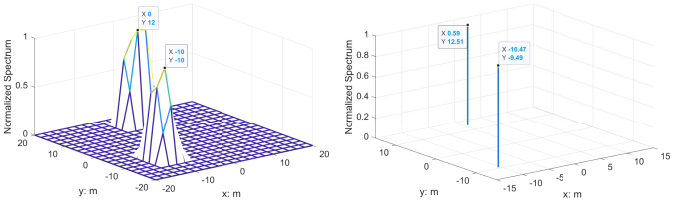

(a) The first step. **(b)** The second step.

Fig. 2. Spatial spectra of the proposed method.

Next, performances of the three methods are evaluated with different SNR values ranging from 0 dB to 20 dB in terms of the root mean square error (RMSE) in the absence of phase error. The results are shown in Fig. 3, with each point obtained by averaging over 100 trials. It can be observed that, although all methods achieve more accurate results with increasing SNR, the method with full coherent measurements consistently outperforms those with magnitude-only ones, especially when the noise level is high. This is not surprising since only magnitude information is used in the non-coherent scenario, and the coherent method effectively provides a performance floor (in terms of RMSE, like some kind of practical "CRB") when phase error is zero. Under the non-coherent scenario, the off-grid model clearly outperforms the on-grid model even when the on-grid model has a denser grid; moreover, the improvement achieved by a denser grid for the proposed off-grid method is not significant. In addition, the proposed non-coherent off-grid method with a 2m stepsize has a better performance than the non-coherent grid-refinement method.

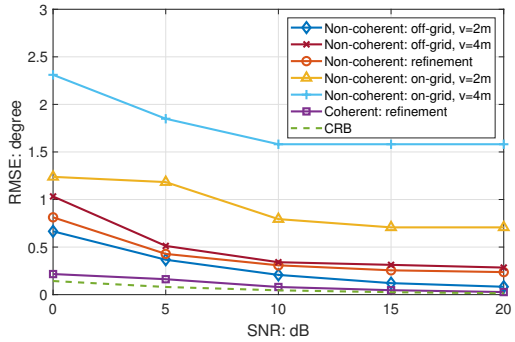

Fig. 3. RMSEs versus SNRs.

Then, we examine the performance in the presence of sensor phase errors. The array measurements with phase error is modelled as $\mathbf{Z}_d = |\mathbf{E}_d\mathbf{A}_d\mathbf{S}_d| + \mathbf{N}_d$, where $\mathbf{E}_d$ is an $M_d \times M_d$ diagonal matrix with each entry being unit complex variable with a random phase term generated independently from the Gaussian distribution with standard derivation σ, representing the phase errors at the d-th array. RMSE results are obtained with an average of 100 trials and the SNR is fixed at 20 dB. As shown in the figure, the proposed non-coherent methods are not affected by phase errors, with a steady performance; on the other hand, the performance of the coherent method declines as the intensity of phase errors increases and becomes much worse than the non-coherent methods when the standard deviation σ of the phase error is larger than 0.15, and in this case, the proposed non-coherent methods are preferred.

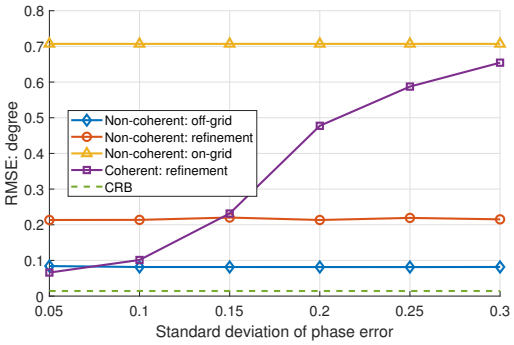

Fig. 4. RMSEs versus sensor phase error.

To evaluate the performance for different number of snapshots, the RMSE results with phase error $\sigma = 0$ and $\sigma = 0.2$ are presented in Fig. 5, with SNR set to be 20dB. Clearly, a larger number of snapshots yield more accurate results and the coherent method consistently outperforms the non-coherent one in the absence of phase errors. However, in the presence of phase errors, the coherent method suffers from a much larger RMSE.

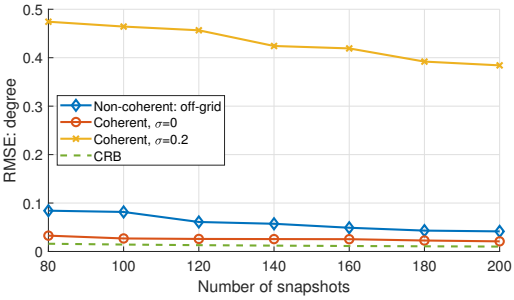

Fig. 5. RMSEs versus number of snapshots.

Finally, the computational complexity is compared in terms of running time, and the results are shown in Table 1, based on a computer with 4.2GHz CPU i7-7700K and 16GB RAM. We can see that although the computational time of off-grid method is higher than the on-grid method, the time cost by the second step of the off-grid model is minimal, especially compared with the refinement method.

Table I: Running time of different non-coherent methods.

Snapshots	On-grid (s)	Off-grid (s)	Refinement (s)
100	226.11	226.22	395.84

V. Conclusions

A novel source localization method with magnitude-only measurements based on distributed array networks has been

proposed. The non-coherent source localization problem was first formulated into a joint sparse phase retrieval form, and the $l_{2,1}$ norm is employed to enforce spatial sparsity, while to tackle the off-grid problem in the second step, dictionary bias is estimated through an iterative process with closed-form solutions at each iteration. As phase error at sensor arrays has no effect on the proposed solution, phase calibration is no longer required. Furthermore, the proposed off-grid method has provided more accurate results than the on-grid method with marginal computational cost, which is significantly less than the widely adopted grid-refinement approach.

REFERENCES

[1] C. Liu, D. Fang, Z. Yang, H. Jiang, X. Chen, W. Wang, T. Xing, and L. Cai, "RSS distribution-based passive localization and its application in sensor networks," *IEEE Trans. Wireless Commun.*, vol. 15, no. 4, pp. 2883–2895, Apr. 2016.

[2] H. Ketabalian, M. Biguesh, and A. Sheikhi, "A closed-fform solution for localization based on RSS," *IEEE Trans. Aerosp. Electron. Syst.*, vol. 56, no. 2, pp. 912–923, Apr. 2020.

[3] D. Dardari, C. Chong, and M. Win, "Threshold-based time-of-arrival estimators in UWB dense multipath channels," *IEEE Trans. Commun.*, vol. 56, no. 8, pp. 1366–1378, Aug. 2008.

[4] R. Amiri, F. Behnia, and A. Noroozi, "An efficient estimator for TDOA-based source localization with minimum number of sensors," *IEEE Commun. Lett.*, vol. 22, no. 12, pp. 2499–2502, Dec. 2018.

[5] Y. Zou, Q. Wan, and H. Liu, "Semidefinite programming for TDOA localization with locally synchronized anchor nodes," in *Proc. IEEE Int. Conf. Acoust., Speech, Signal Process.*, Calgary, Canada, Apr. 2016, pp. 3524–3528.

[6] Z. Dai, G. Wang, and H. Chen, "Sensor selection for TDOA-based source localization using angle and range information," *IEEE Trans. Aerosp. Electron. Syst.*, vol. 57, no. 4, pp. 2597–2604, Feb. 2021.

[7] A. J. Weiss, "Direct position determination of narrowband radio frequency transmitters," *IEEE Signal Process. Lett.*, vol. 11, no. 5, pp. 513–516, May 2004.

[8] N. Garcia, H. Wymeersch, E. G. Larsson, A. M. Haimovich, and M. Coulon, "Direct localization for massive MIMO," *IEEE Trans. Signal Process.*, vol. 65, no. 10, pp. 2475–2487, May 2017.

[9] K. Dogancay, "Bearings-only target localization using total least squares," *Signal Process.*, vol. 85, no. 9, pp. 1695–1710, Apr. 2005.

[10] Z. Wang, J. Luo, and X. Zhang, "A novel location-penalized maximum likelihood estimator for bearing-only target localization," *IEEE Trans. Signal Process.*, vol. 60, no. 12, pp. 6166–6181, Dec. 2012.

[11] R. Schmidt, "Multiple emitter location and signal parameter estimation," *IEEE Trans. Antennas Propag.*, vol. 34, no. 3, pp. 276–280, Mar. 1986.

[12] R. Roy and T. Kailath, "ESPRIT, estimation of signal parameters via rotation invariance techniques," *IEEE Trans. Acoust., Speech, Signal Process.*, vol. 37, no. 7, pp. 984–995, Jul. 1989.

[13] D. Malioutov, M. Cetin, and S. Willsky, "A sparse signal reconstruction perspective for source localization with sensor arrays," *IEEE Trans. Signal Process.*, vol. 53, no. 8, pp. 3010–3022, Aug. 2005.

[14] Q. Shen, W. Liu, L. Wang, and Y. Liu, "Group sparsity based localization for far-field and near-field sources based on distributed sensor array networks," *IEEE Trans. Signal Process.*, vol. 68, pp. 6493–6508, Nov. 2020.

[15] M. Delbari, A. Javaheri, H. Zayyani, and F. Marvasti, "Non-coherent DOA estimation via majorization-minimization using sign information," *IEEE Signal Process. Lett.*, vol. 29, pp. 892–896, Mar. 2022.

[16] H. Kim, A. M. Haimovich, and Y. C. Eldar, "Non-coherent direction of arrival estimation from magnitude only measurements," *IEEE Signal Process. Lett.*, vol. 22, no. 7, pp. 925–929, Jul. 2015.

[17] H. Zayyani and M. Korki, "Non-coherent direction of arrival estimation via frequency estimation," 2016, doi:arXiv:1606.06423.

[18] W. Wang, R. Wu, J. Liang, and H. C. So, "Phase retrieval approach for DOA estimation with array errors," *IEEE Trans. Aerosp. Electron. Syst.*, vol. 53, no. 5, pp. 2610–2620, May 2017.

[19] C. R. Karanam, B. Korany, and Y. Mostofi, "Magnitude-based angle-of-arrival estimation, localization, and target tracking," in *Proc. ACM/IEEE Int. Conf. Inf. Process. Sens. Netw.*, Porto, Portugal, Apr. 2018, pp. 254–265.

[20] Y. Tian, J. Shi, Y. Wang, and Q. Lian, "Non-coherent direction of arrival estimation utilizing linear model approximation," *Signal Process.*, vol. 157, pp. 261–265, Dec. 2019.

[21] Z. Wan and W. Liu, "Non-coherent DOA estimation via proximal gradient based on a dual-array structure," *IEEE Access*, vol. 9, pp. 26 792–26 801, Feb. 2021.

[22] H. Huang, S. H. C., and Z. A. M., "Off-grid direction-of-arrival estimation using second-order taylor approximation," *Signal Process.*, vol. 196, pp. 1–4, Jul. 2022.

[23] Z. Wan, W. Liu, and P. Willett, "Non-coherent source localization with distributed sensor arrays," in *Proc. IEEE Sensor Array and Multichannel Signal Processing Workshop*, Trondheim, Norway, Jun. 2022.

[24] Z. Wan and W. Liu, "Non-coherent DOA estimation of off-grid signals with uniform circular arrays," in *Proc. IEEE Int. Conf. Acoust., Speech, Signal Process.*, Toronto, Canada, Apr. 2021, pp. 4370–4374.

[25] Z. Yang, L. Xie, and C. Zhang, "Off-grid direction of arrival estimation using sparse Bayesian inference," *IEEE Trans. Signal Process.*, vol. 61, no. 1, pp. 38–43, Oct. 2013.

[26] X. Wu, W. Zhu, J. Yan, and Z. Zhang, "Two sparse-based methods for off-grid direction-of-arrival estimation," *Signal Process.*, vol. 142, pp. 87–95, Jan. 2018.

[27] Q. Shen, W. Cui, W. Liu, S. Wu, Y. D. Zhang, and M. G. Amin, "Underdetermined wideband DOA estimation of off-grid sources employing the difference co-array concept," *Signal Process.*, vol. 130, pp. 299–304, Jul. 2016.

[28] H. Zhu, G. Leus, and G. B. Giannakis, "Sparsity-cognizant total least-squares for perturbed compressive sampling," *IEEE Trans. Signal Process.*, vol. 59, no. 5, pp. 2002–2016, February 2011.

[29] W. Liu, "Blind adaptive wideband beamforming for circular arrays based on phase mode transformation," *Digit. Signal Process.*, vol. 21, pp. 239–247, Mar. 2011.

[30] T. Qiu, P. Babu, and D. P. Palomar, "Prime: Phase retrieval via majorization-minimization," *IEEE Transactions on Signal Processing*, vol. 64, no. 19, pp. 5174–5186, Jun. 2016.

[31] Q. Chen, N. D. Sidiropoulos, K. Huang, L. Huang, and S. H. C., "Phase retrieval using feasible point pursuit: algorithms and Cramer–Rao bound," *IEEE Trans. Signal Process.*, vol. 64, no. 20, pp. 5282–5296, Oct. 2016.

[32] Y. Liang, W. Liu, Q. Shen, W. Cui, and S. Wu, "A review of closed-form cramér-rao bounds for DOA estimation in the presence of Gaussian noise under a unified framework," *IEEE Access*, vol. 8, pp. 175 101–175 124, Sep. 2020.

[33] S. M. Kay, *Fundamentals of Statistical Signal Processing: Estimation Theory*. NJ: Upper Saddle River, 1993.